



Coadsorption and subsequent redox conversion behaviors of As(III) and Cr(VI) on Al-containing ferrihydrite[☆]



Zecong Ding^a, Fenglian Fu^{a, *}, Dionysios D. Dionysiou^b, Bing Tang^a

^a School of Environmental Science and Engineering and Institute of Environmental Health and Pollution Control, Guangdong University of Technology, Guangzhou 510006, China

^b Environmental Engineering and Science Program, Department of Biomedical, Chemical and Environmental Engineering (DBCEE), University of Cincinnati, OH 45221-0012, USA

ARTICLE INFO

Article history:

Received 15 September 2017

Received in revised form

13 November 2017

Accepted 28 December 2017

Available online 12 January 2018

Keywords:

As(III)

Cr(VI)

Al-containing ferrihydrite

Coadsorption

Redox

ABSTRACT

Naturally occurring ferrihydrite often contains various impurities, and Al is one of the most prominent impurities. However, little is known about how these impurities impact the physical and chemical properties of ferrihydrite with respect to metal(loid) adsorption. In this study, a series of Al-containing ferrihydrites were synthesized and exposed to a mixed solution containing As(III) and Cr(VI). The results showed that the two contaminants can be quickly adsorbed onto the surface of Al-containing ferrihydrite under acidic and neutral conditions. With the increase of Al molar percentage in ferrihydrites from 0 to 30, the adsorption capacity of As(III) decreased, whereas it increased for Cr(VI). On the other hand, with the increase of pH value from 3.0 to 11.0, the decreasing rate of As(III) was accelerated first, then slowed down, whereas the Cr(VI) decreasing rate slowed down dramatically. X-ray diffraction (XRD), Brunauer-Emmett-Teller (BET) analysis method, transmission electron microscopy (TEM) analysis, energy dispersive spectroscopy (EDS) mapping, Attenuated Total Reflectance Fourier Transform Infrared Spectroscopy (ATR-FTIR), and X-ray photoelectron spectroscopy (XPS) were employed to characterize Al-containing ferrihydrite. Interestingly, it was found that the redox transformation occurred between As(III) and Cr(VI) after the two contaminants were coadsorbed onto the surface of Al-containing ferrihydrite. The oxidation of As(III) to As(V) and reduction of Cr(VI) to Cr(III) would greatly lower the environmental hazard of the As(III) and Cr(VI).

© 2018 Elsevier Ltd. All rights reserved.

1. Introduction

Iron (hydr)oxides are often found in the natural environment, and they play an important role in the remediation of environmental contaminants (Zhou et al., 2014; Tang et al., 2017). Ferrihydrite is an environmentally important iron (hydr)oxides commonly found in soils, sediments, and often in areas contaminated by acid mine drainage (Jambor and Dutrizac, 1998; Michel et al., 2007). Due to its abundance in nature, high surface area and content of reactive surface groups (Filip et al., 2007; Meng et al., 2014), ferrihydrite plays an important role in affecting the migration and transformation of contaminants in aquatic environments through adsorption (Qi and Pichler, 2016), coprecipitation (Martin

et al., 2005), and redox reactions (Fortin and Langley, 2005). Ferrihydrite is a particularly effective adsorbent for both arsenic (Zhu et al., 2011) and heavy-metal ions (Karapinar, 2016), and hence, ferrihydrite is manufactured for use in wastewater treatment (Smith et al., 2012). However, in natural environments, ferrihydrite is rarely found as a pure phase and instead often contains foreign ions, especially Al (Adra et al., 2016). Al is the third most abundant element in the Earth's crust (Casey, 2006), and it is often found in the structure of Fe (hydr)oxides such as maghemite (up to 10 mol% Al), hematite (up to 18 mol% Al), and goethite (up to 33 mol% Al) (Cismasu et al., 2012). In the case of Al-containing ferrihydrite, it was reported that Al element can be incorporated in the ferrihydrite structure up to 30 mol% (Johnston and Chrysochoou, 2016). It has been shown that the occurrence of Al affects the physico-chemical properties of ferrihydrite, such as particle morphology and size, solubility, and redox (Cismasu et al., 2012, 2013; Johnston and Chrysochoou, 2016). Besides, with the increase of Al content from 0 to 13 mol%, bacterial Fe(III) reduction rates of Al-containing

[☆] This paper has been recommended for acceptance by Joerg Rinklebe.

* Corresponding author.

E-mail address: fufenglian2006@163.com (F. Fu).

ferrihydrate significantly decreased (Ekstrom et al., 2010), which indicates that Al-containing ferrihydrate can exist in more stable forms in natural environment than pure ferrihydrate.

Due to the widespread occurrence and toxicity, arsenic and chromium are listed as priority hazardous substance by the United States Environmental Protection Agency (de Oliveira et al., 2014). Arsenic is mainly present in inorganic forms in natural water, and occurs as arsenite (As(III)) and arsenate (As(V)) (Sorg et al., 2014). As(III) is dominant in groundwater due to the anoxic condition, while As(V) is primarily present in well-oxygenated water. As(III) exists as an uncharged species (H_3AsO_3) at pH values below 9.2 and as H_2AsO_3^- at a pH range of 9.2–12.1, while As(V) often occurs as oxyanions (H_2AsO_4^- and HAsO_4^{2-}) in a pH range of about 2.1–11.9 (Smedley and Kinniburgh, 2002). Although both As(III) and As(V) are toxic and carcinogenic to human beings (Nordstrom, 2002), As(III) is considered much more toxic, more soluble, and more mobile than As(V) (Zhang et al., 2007). Chromium, another common contaminant, is involved in many industries including metallurgy, electroplating, leather tanning, dye and pigment (Kimbrough et al., 1999). In general, chromium exists in the environment as trivalent (Cr(III)) and hexavalent (Cr(VI)) species. The toxic Cr(VI) occurs mainly as oxyanions (HCrO_4^- and CrO_4^{2-}) at low concentration and pH higher than 3 (Kotaš and Stasicka, 2000), while Cr(III) is less toxic and can be effectively immobilized as the hydroxide ($\text{Cr}(\text{OH})_3$) in the pH range of ~6–11.5 (Cerkez et al., 2015). Cr(VI) is carcinogenic and mutagenic to human beings, and its toxicity is due to its high solubility in water and rapid permeability through biological membranes (Levina et al., 2003).

Ferrihydrate is one of the most important mineral adsorbents to control the fate of As(III) and Cr(VI). Zhao et al. (2011) pointed out that As(III) can be adsorbed onto the surface of ferrihydrate and can be oxidized to As(V) by dissolved oxygen. Spectroscopic study indicated that Cr(VI) can form inner-sphere complexes on ferrihydrate (Johnston and Chrysochoou, 2012). In the environment, As(III) and Cr(VI) can be found in a variety of settings, including soil, groundwater, and many industrial wastewaters, especially in acid mine drainage (Le Hécho et al., 2003). Cerkez et al. (2015) used ferrihydrate as an adsorbent for simultaneous removal of As(III) and Cr(VI), and they observed a significant phenomenon that As(III) and Cr(VI) converted to lower toxicity species, As(V) and Cr(III). The overall redox reaction between As(III) and Cr(VI) can be described as Eq. (1).



However, when Al incorporated into ferrihydrate, how does Al-containing ferrihydrate interact with As(III) and Cr(VI)? Whether the incorporation of Al will affect the adsorption of As(III) and Cr(VI), as well as the redox conversion between the two contaminants? In this paper, further researches have been studied. A series of Al-containing ferrihydrates were prepared by co-precipitation, and were exposed to a mixed solution containing As(III) and Cr(VI). Batch experiments were carried out to examine the removal performance of As(III) and Cr(VI) by Al-containing ferrihydrate. The experimental parameters affecting the removal of As(III) and Cr(VI) by Al-containing ferrihydrate were investigated and the reaction mechanisms were discussed.

2. Materials and methods

2.1. Chemicals

All the chemicals were at least of analytical grade, and all solutions were prepared with deionized water. NaAsO_2 and $\text{K}_2\text{Cr}_2\text{O}_7$ were used to prepared As(III) and Cr(VI) stock solution,

respectively. Mixed solution of As(III) and Cr(VI) were freshly prepared.

2.2. Synthesis of Al-containing ferrihydrate

Al-containing ferrihydrate was synthesized according to a modified version of the method adopted by Cismasu et al. (2012). Briefly, stock solutions of $\text{Fe}(\text{NO}_3)_3$ and $\text{Al}(\text{NO}_3)_3$ were combined to obtain 100 mL solutions with a total concentration of $([\text{Fe}^{3+}] + [\text{Al}^{3+}])$ of 0.2 mol/L in proportions corresponding to 0, 10, 20, and 30 mol% Al, respectively. These solutions were adjusted to pH 7.5 by adding dropwise 1.0 mol/L NaOH under magnetic stirring. All suspensions were centrifuged after pH neutralization and the solids were washed repeatedly with deionized water to remove excess electrolytes. The washed materials were freeze-dried for 8 h before being ground into fine powders, and the final products were stored in 4 °C freezer. The Al-containing ferrihydrate samples obtained by this procedure had 0, 10, 20, and 30 mol% Al, and were referred to as Fh-Al-0, Fh-Al-10, Fh-Al-20, and Fh-Al-30, respectively. The morphologies of the four samples were observed by scanning electron microscopy (SEM) image analysis (Fig. S1).

2.3. Coexistence of As(III) and Cr(VI)

Defined amounts of As(III) and Cr(VI) stock solutions were added into a 500 mL conical flask, to obtain a mixed solution (200 mL) containing 150 $\mu\text{mol/L}$ As(III) and 100 $\mu\text{mol/L}$ Cr(VI). The initial pH of the mixed solutions were adjusted to the designated values (3.0, 7.0, and 11.0) with HCl solution (0.1–1 mol/L) or NaOH solution (0.1–1 mol/L). All conical flasks were shaken on a thermostatic shaker (120 ± 5 rpm) at 25 ± 1 °C. No acid or alkali was subsequently added to control the pH during the reaction. After 24 h, the residual concentrations of As(III) and Cr(VI) were determined.

2.4. Simultaneous removal of As(III) and Cr(VI)

Al-containing ferrihydrates with different Al content (1.5 g/L) were added into the mixed solutions (containing 150 $\mu\text{mol/L}$ As(III) and 100 $\mu\text{mol/L}$ Cr(VI)) at various initial pH values (3.0, 7.0, and 11.0). All the mixed solutions were shaken on a thermostatic shaker (120 ± 5 rpm) at 25 ± 1 °C. Appropriate amounts of suspensions were taken from the conical flask at 5, 10, 20, 30, 45, 60, 90, and 120 min of reaction, and the suspensions were filtered through a 0.45 μm membrane filter. The residual concentrations of As(III) and Cr(VI), as well as the possible generated As(V) and Cr(III) in the filtered solution were determined.

2.5. Adsorption isotherm

To obtain the adsorption isotherms, 0.1 g Al-containing ferrihydrates were exposed to 100 mL solutions ($\text{pH}_0 = 3.0$) containing different concentrations of As(III) or Cr(VI). Initial As(III) concentrations ranged from 300 to 1800 $\mu\text{mol/L}$, while initial Cr(VI) concentrations ranged from 400 to 4000 $\mu\text{mol/L}$. The mixtures were shaken on a thermostatic shaker (120 ± 5 rpm) at 25 ± 1 °C for 24 h. The equilibrium adsorption capacity (q_e) ($\mu\text{mol/g}$) for As(III) or Cr(VI) was calculated according to Eq. (2).

$$q_e = \frac{(C_0 - C_e)V}{m} \quad (2)$$

where C_0 ($\mu\text{mol/L}$) is the initial concentrations of As(III) or Cr(VI), and C_e ($\mu\text{mol/L}$) is the equilibrium concentrations of As(III) or Cr(VI), and V (L) is the volume of As(III) or Cr(VI) solutions, and m

(g) is the mass of Al-containing ferrihydrites.

Langmuir (Eq. (3)) and Freundlich (Eq. (4)) isotherms were employed to study the adsorption of As(III) or Cr(VI) on Al-containing ferrihydrites.

$$q_e = \frac{q_{\max} K_L C_e}{1 + K_L C_e} \quad (3)$$

$$q_e = K_F C_e^{1/n} \quad (4)$$

where q_e ($\mu\text{mol/g}$) is the equilibrium adsorption capacity of the adsorbents, q_{\max} ($\mu\text{mol/g}$) is the maximum adsorption capacity, K_L ($\text{L}/\mu\text{mol}$) is a Langmuir constant related to the affinity of the binding sites and energy of adsorption in Eq. (3), whereas K_F ($\mu\text{mol/g}(\text{L}/\mu\text{mol})^{1/n}$) is the adsorption capacity of the adsorbents, and n is the adsorption intensity in Eq. (4).

2.6. Desorption experiments

Desorption tests were carried out using 1.0 mol/L NaOH solution. First, the Al-containing ferrihydrites were exposed to a mixed solution (100 mL) containing 150 $\mu\text{mol/L}$ As(III) and 100 $\mu\text{mol/L}$ Cr(VI) under the initial pH 3.0 for 2.0 h. The Al-containing ferrihydrites after reaction were collected and mixed with 100 mL 1.0 mol/L NaOH solution, and the mixture was shaken for 3.0 h. After filtration, the concentrations of As(III), As(V), Cr(VI), and Cr(III) in the filtered solution were determined.

2.7. Determination of As(III), As(V), Cr(VI) and Cr(III) concentration

According to the adapted method from Kim and Choi (2011), the As(V) concentrations were measured spectrophotometrically using molybdenum blue method. The concentrations of total As (As(V) + As(III)) were determined by a hydride generation-dual channel atom fluorescence spectrometer (HG-AFS, AF-640A, Beijing Rayleigh Analytic Instrument Co., Beijing, China). The As(III) concentrations were calculated as the difference between the total As and As(V) concentrations. The concentrations of Cr(VI) were measured spectrophotometrically at 540 nm using 1,5-diphenylcarbazide as the complexing agent (Kim and Choi, 2011). The total Cr (Cr(VI) + Cr(III)) concentrations were determined by a flame atomic absorbance spectrometer (AAS, Z-2000, Hitachi, Japan). The concentrations of Cr(III) were calculated as the difference between the total Cr and Cr(VI) concentrations.

2.8. Characterization methods

XRD patterns of Al-containing ferrihydrites were recorded using an X-ray powder diffractometer (XD-2, Purkinje General Instrument Co., Ltd., China) with Cu $K\alpha$ radiation. The morphologies of Al-containing ferrihydrites were observed by an SU8010 SEM (Hitachi SU8010, Japan). Transmission electron microscopy (TEM) and high-resolution transmission electron microscopy (HR-TEM) images were carried out on a FEI Tecnai G2 F20 S-Twin microscope with a field emission gun operating at 200 kV. The transmission electron microscope is equipped with an energy dispersive spectroscopy (EDS) detector, which was used for elemental analysis of the samples. The specific surface areas of the Al-containing ferrihydrites were determined by Brunauer-Emmett-Teller (BET) N_2 adsorption analysis using a surface area analyzer (Nova, 2000e; Quantachrome Instrument, USA). The pore size distribution and pore volume were derived from the Barrett-Joyner-Halenda (BJH) model. Attenuated Total Reflectance Fourier Transform Infrared Spectroscopy (ATR-

FTIR) spectral measurements of the samples were collected using a Tensor 27 Bruker FTIR system with an ATR accessory. The X-ray photoelectron spectroscopy (XPS) studies of the Al-containing ferrihydrite before and after reaction were performed using an Amicus (Shimadzu Co., Japan) X-ray photoelectron spectroscopy with normal Al $K\alpha$ radiation (1486.8 eV) under a residual pressure of 2×10^{-9} Torr. A small amount of Al-containing ferrihydrites were pressed onto conductive carbon tape for XPS measurements. The binding energies from the samples were calibrated with respect to the C 1s peak from the carbon tape at 284.6 eV. The XPS data were analyzed using XPSPEAK 41 software.

3. Results and discussion

3.1. Coexistence of As(III) and Cr(VI)

First, As(III) and Cr(VI) were mixed together to investigate whether the direct redox would happen between the two contaminants in aqueous solution (in the absence of Al-containing ferrihydrite). As shown in Fig. S2, after 24 h, the final concentrations of As(III) and Cr(VI) did not change compared with their initial concentrations at pH 3.0, 7.0, and 11.0. This result indicated that As(III) and Cr(VI) can coexist stably in aqueous solution under the conditions of no other foreign substances adding or no energy applying to the system, being consistent with the results reported by Cerkez et al. (2015).

3.2. Characterizations of Al-containing ferrihydrite

3.2.1. XRD

The XRD patterns of Al-containing ferrihydrites are shown in Fig. 1. The Fh-Al-0 showed two broad and weak peaks at 2θ of 35 and 62°, being consistent with the XRD of 2-line ferrihydrite, which belonged to poorly crystalline ferrihydrite (Liu et al., 2016a). Increasing Al content to 30 mol% causes essentially no changes in peak positions for Al-containing ferrihydrite. According to the study by Adra et al. (2016), when the Al content increases to 39 mol% in ferrihydrite, the presence of gibbsite ($\alpha\text{-Al}(\text{OH})_3$) can be observed by XRD analyses. In this paper, no $\alpha\text{-Al}(\text{OH})_3$ was detected by XRD analyses, which indicated that Al^{3+} may substitute for Fe^{3+}

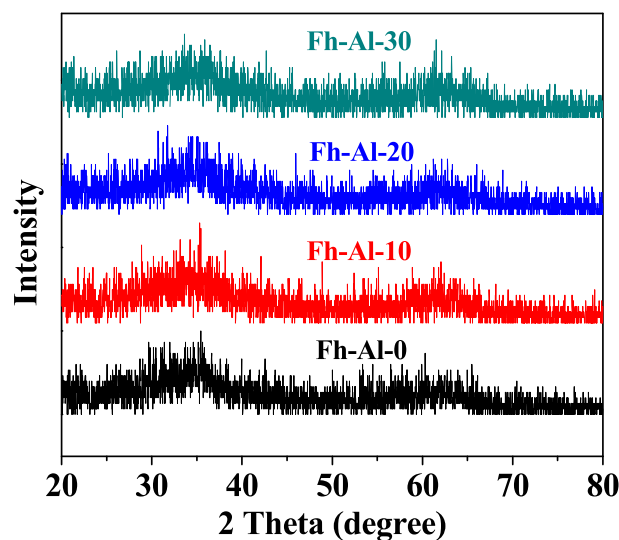


Fig. 1. XRD patterns of the four Al-containing ferrihydrites.

in the structure of these synthetic Al-containing ferrihydrite samples.

3.2.2. TEM

In order to further observe the morphologies of Al-containing ferrihydrite, TEM images were collected for Fh-Al-30 (Fig. S3). Images obtained for Fh-Al-30 indicated that the sample consisted of numbers of nanoparticles, and these nanoparticles were aggregated to form large agglomerates. However, plenty of voids and interspaces are present among the nanoparticles, which may increase the surface areas of the sample. In the HR-TEM, no obvious lattice fringe was observed, which indicated that Fh-Al-30 was a poor crystallinity material. The TEM and HR-TEM images of Fh-Al-0 were also collected and discussed in Fig. S3.

3.2.3. BET

In order to characterize the specific surface areas and porous structures of Fh-Al-30, N₂ adsorption analysis was carried out. Fig. S4 presents the N₂ adsorption-desorption isotherms and BJH pore size distribution curves of the Al-containing ferrihydrite. The result showed that Fh-Al-30 possessed a large surface area of 269.5 m²/g, and its pore volume was 0.188 cm³/g. The pore size distribution of Fh-Al-30 showed that the sample had an average pore width of 3.6 nm, indicating the mesoporous structure of the sample. It can be reasonably hypothesized that the large BET surface area and pore volume of this sample can improve the accessibility of active sites for As(III) and Cr(VI), contributing to great adsorption capacities for the two contaminants. N₂ adsorption analysis of Fh-Al-0 was also carried out and discussed in Fig. S4.

3.3. Simultaneous removal of As(III) and Cr(VI)

3.3.1. Effect of Al content

The concentrations of As(III), As(V), Cr(VI), and Cr(III) in aqueous phase were simultaneously monitored with time for ferrihydrites with different Al content (Fig. 2). For Fh-Al-0, at pH 3.0, the As(III) concentration decreased from initial 150.0 μmol/L to 13.1 μmol/L within 20 min, reaching more than 90% removal. This great removal efficiency of As(III) by ferrihydrite had also been reported by Zhao et al. (2011). On the other hand, the residual concentration of Cr(VI) decreased much faster than that of As(III) under the condition of pH 3.0. After reaction for 5 min, Cr(VI) concentration decreased from initial 100.0 μmol/L to 3.2 μmol/L, indicating almost complete removal of Cr(VI) from solution.

From Fig. 2(a)–(d), it can be found that with an increase of Al content in ferrihydrites, the rate of decrease in As(III) concentration slowed down. However, approximately 97% of As(III) was removed within 2 h by Fh-Al-30. On the other hand, under the condition of pH 3.0, the concentration of Cr(VI) decreased rapidly, and was below the detection limit of Cr(VI), 0.078 μmol/L, after reaction for 30 min. According to previous studies (Zhao et al., 2011; Johnston and Chrysochoou, 2016), both As(III) and Cr(VI) can be removed from aqueous phase via forming complexes on ferrihydrite. The rapid decrease of As(III) and Cr(VI) concentration may be attributed to the complexation of the two contaminants with the -OH on the surface of Al-containing ferrihydrite (Eqs. (5) and (6)). The -OH on the surface of Al-containing ferrihydrite will be discussed later in XPS analysis.

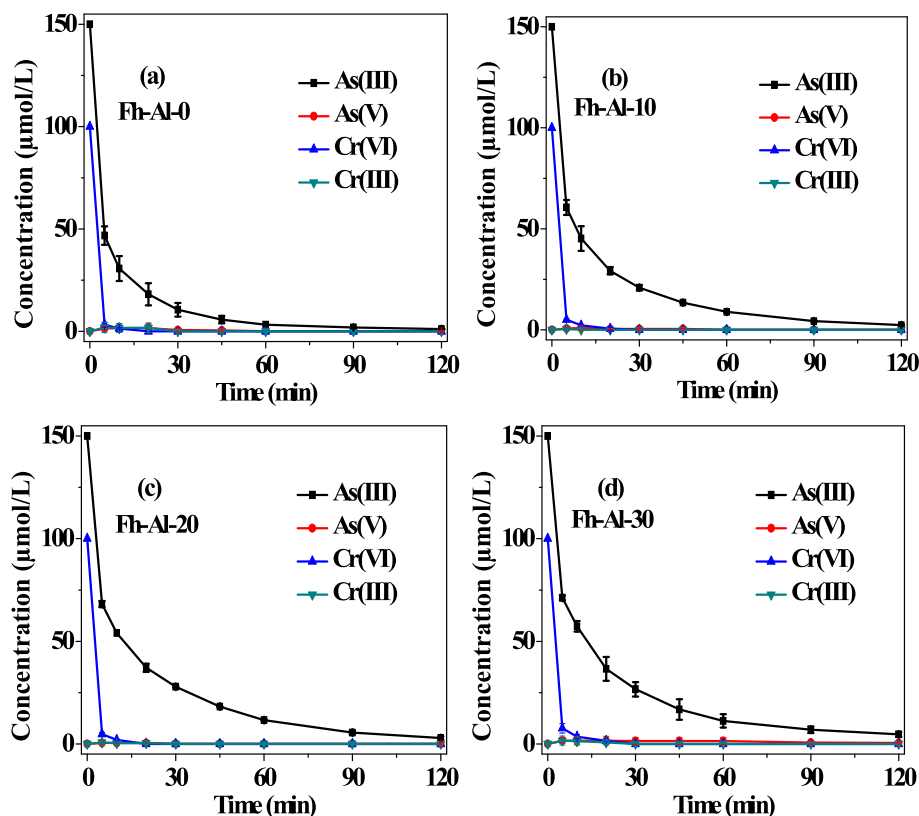
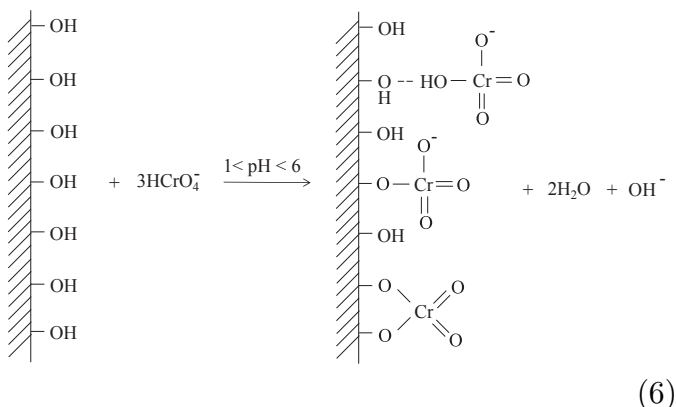
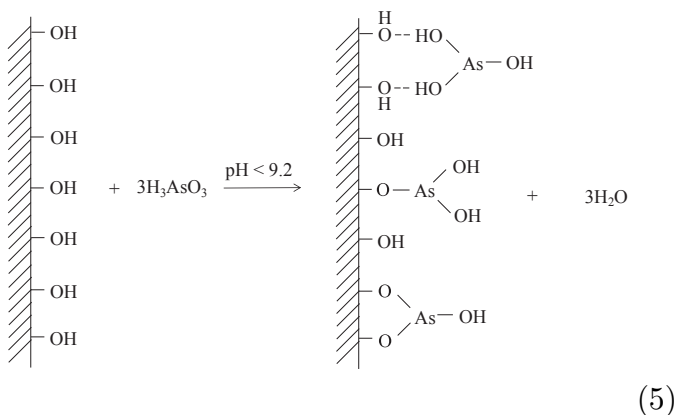


Fig. 2. The concentration profiles of As(III), As(V), Cr(VI), and Cr(III) in the simultaneous removal of As(III) and Cr(VI) by (a) Fh-Al-0, (b) Fh-Al-10, (c) Fh-Al-20, and (d) Fh-Al-30 (pH₀ = 3.0, [As(III)]₀ = 150 μmol/L, [Cr(VI)]₀ = 100 μmol/L, [Al-containing ferrihydrite]₀ = 1.5 g/L).



In the four Al-containing ferrihydrites reaction systems, the concentrations of As(V) and Cr(III) in aqueous phase were nearly undetectable (Fig. 2(a)–(d)). The concentrations of dissolved oxygen in the reaction systems were investigated (Fig. S5).

3.3.2. Effect of initial pH

The effect of initial pH on the removal of As(III) and Cr(VI) by Fh-Al-0 and Fh-Al-30 was investigated (Fig. 3). As for Cr(VI), the concentration was evidently dependent on pH value. In the Fh-Al-0 system, after reaction for 30 min, the residual Cr(VI) concentrations were 0, 9.9, and 95.6 $\mu\text{mol/L}$ at initial pH 3.0, 7.0, and 11.0, respectively. This similar pH dependence of Cr(VI) removal was also found in the Fh-Al-30 system. These results showed that the greatest removal efficiency of Cr(VI) occurred at pH 3.0, and the Cr(VI) removal efficiency decreased with the increase of pH. The reason may be attributed to the electrostatic interaction between Al-containing ferrihydrite and Cr(VI). Cismasu et al. (2013) found that the point of zero charge (pH_{PZC}) of Al-containing ferrihydrite increased from 8.5 to 9.0 with increasing Al content from 0 to 20 mol% Al. The surface of adsorbents carried a positive charge when the pH was below their pH_{PZC} and a negative charge when the pH was above their pH_{PZC} . Since the Cr(VI) exists primarily as negative species (HCrO_4^- and CrO_4^{2-}) under designed pH (3.0–11.0), the removal of Cr(VI) can achieve a highest efficiency at pH 3.0 due to the electrostatic attraction between the negative Cr(VI) species and the positively charged Al-containing ferrihydrite. At pH 11.0, the electric repulsion between Cr(VI) and Al-containing ferrihydrite was unfavorable to Cr(VI) adsorption. The pH dependence of Cr(VI) removal was also reported by Cerkez et al. (2015), and they pointed out that electrostatic interaction was the main reason. The residual concentrations of Cr(VI) decreased so quickly by Fh-Al-0 and Fh-Al-30 at pH 3.0, and it was difficult to distinguish which sample was

preferable. However, under the condition of pH 7.0 and 11.0, the residual concentrations of Cr(VI) decreased faster in the Fh-Al-30 system than in the Fh-Al-0 system. The presence of Al in ferrihydrite increased the affinity of ferrihydrite towards Cr(VI).

As for As(III), the concentrations decreased faster at the initial pH 7.0 than at the initial pH 3.0. The $\text{pK}_{\text{a}1}$ of H_3AsO_3 is 9.2, which indicates that As(III) exists as H_3AsO_3 rather than oxyanions at pH lower than 9.2. This faster decreasing rate of As(III) in pH 7.0 than in pH 3.0 may be attributed to the fact that this increase of pH was favorable for the dissociation of H_3AsO_3 to H_2AsO_3^- . The electrostatic attraction between H_2AsO_3^- and positively charged Al-containing ferrihydrite was favorable the adsorption As(III). However, when the initial pH increased to 11.0, the decreasing rate of As(III) slowed down. Under the condition of initial pH 11.0, the surface of Al-containing ferrihydrite carried a negative charge, and the electric repulsion between As(III) and Al-containing ferrihydrite was unfavorable to As(III) removal. The decreasing rate of As(III) was faster in Fh-Al-0 system than in Fh-Al-30 system, which indicated that 30 mol% Al content in Fh-Al-30 weakened the affinity of ferrihydrite toward As(III). Similar to the above results, concentrations of aqueous As(V) and Cr(III) were still nearly undetectable under the designated pH values.

The effect of As(III)/Cr(VI) molar ratio on the removal of As(III) and Cr(VI) by Fh-Al-0 and Fh-Al-30 was also investigated and discussed (Fig. S6).

3.4. Adsorption isotherms

Both Langmuir and Freundlich models were used to describe the As(III) and Cr(VI) adsorption isotherms (Fig. 4). The adsorption constants obtained from the isotherms are presented in Table 1. As shown in Fig. 4 and Table 1, Langmuir isotherm instead of Freundlich isotherm can describe well the adsorption process of As(III) or Cr(VI) based on the higher regression coefficient (R^2) values. According to the Langmuir isotherm, the Al content in ferrihydrite had contrasted effects on the As(III) and Cr(VI) sorption isotherms. Indeed, with an increase of Al content in ferrihydrite from 0 to 30 mol%, the maximum adsorption capacity (q_m) of As(III) decreased from 1234.1 $\mu\text{mol/g}$ to 867.1 $\mu\text{mol/g}$, while the q_m of Cr(VI) increased from 805.1 $\mu\text{mol/g}$ to 934.1 $\mu\text{mol/g}$. The decrease in As(III) adsorption capacity with increasing Al content in ferrihydrite may be due to a low affinity of the As(III) for Al surface sites comparing with Fe surface sites (Adra et al., 2016). While the increase in Cr(VI) adsorption capacity with increasing Al content in ferrihydrite may be due to a high affinity of Cr(VI) for Al surface sites comparing with Fe surface sites. The presence of Al in ferrihydrite decreased the adsorption capacity of As(III), but increased the Cr(VI) adsorption capacity.

3.5. Desorption studies

As shown in Fig. 5, in addition to As(III) and Cr(VI), both As(V) and Cr(III) were detected in the desorption solutions. The existence of As(III) and Cr(VI) in the desorbed solution indicated that the two contaminants had been adsorbed on the four Al-containing ferrihydrites. While the occurrence of As(V) and Cr(III) indicated that the redox transformation occurred between As(III) and Cr(VI) after the two contaminants were coadsorbed on the surface of Al-containing ferrihydrite.

3.6. Characterizations of Al-containing ferrihydrite after reaction

3.6.1. TEM

After reaction, Fh-Al-30 nanoparticles were strongly aggregated together (Fig. 6). In the TEM-EDS elemental maps of Fh-Al-30, it can

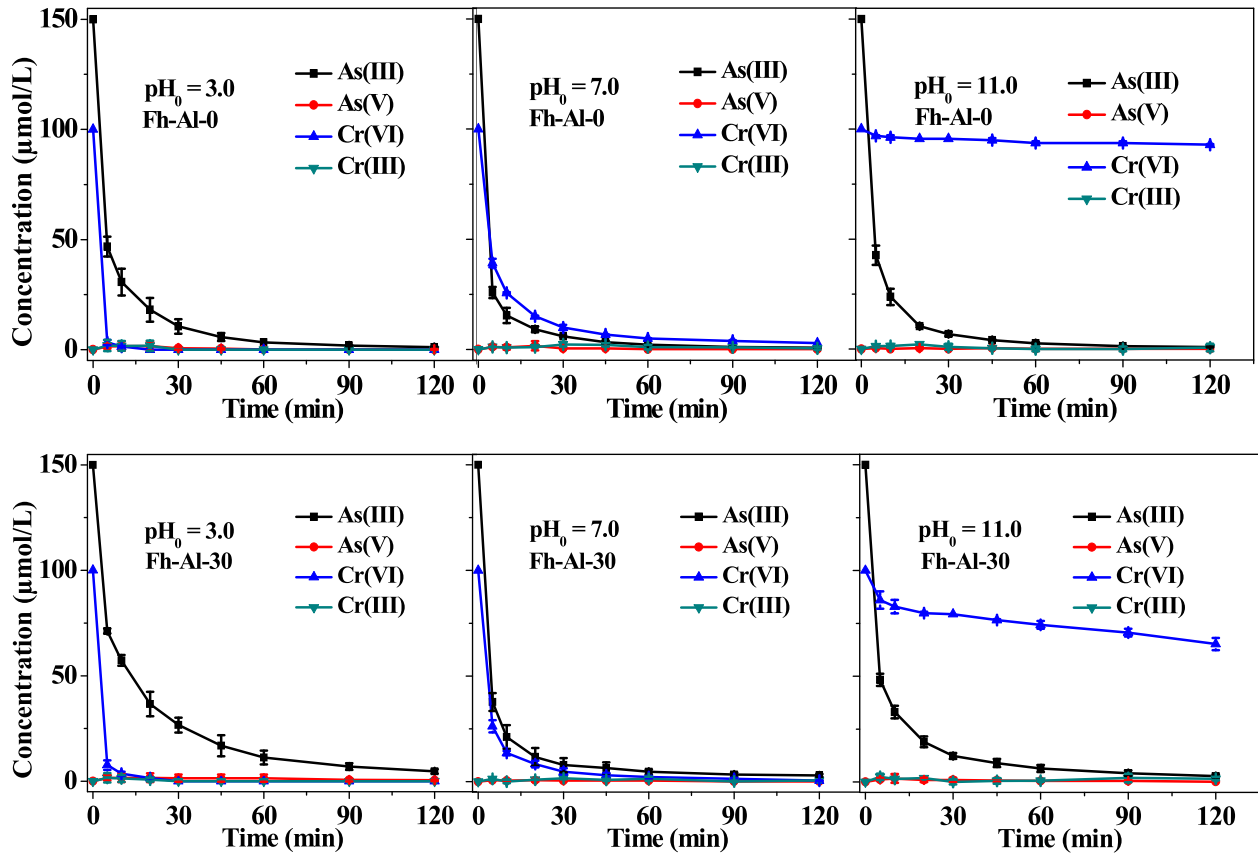


Fig. 3. Effect of initial pH on the removal of As(III) and Cr(VI) by Fh-Al-0 and Fh-Al-30 ($[As(III)]_0 = 150 \mu\text{mol/L}$, $[Cr(VI)]_0 = 100 \mu\text{mol/L}$, $[Al\text{-containing ferrihydrite}]_0 = 1.5 \text{ g/L}$).

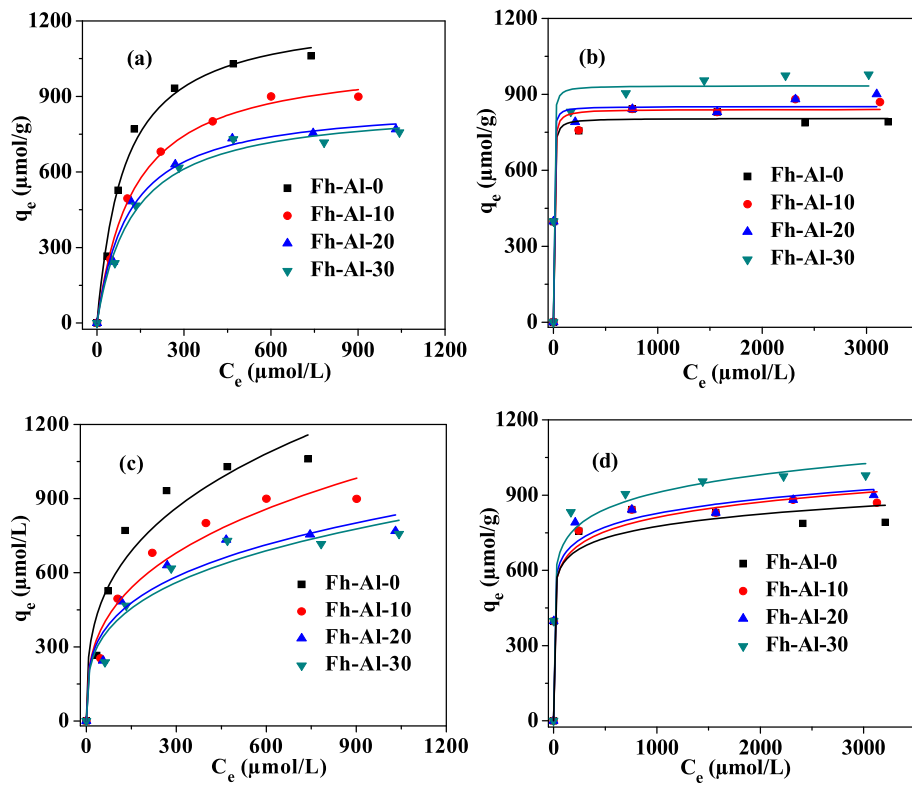


Fig. 4. Langmuir adsorption isotherms for (a) As(III) and (b) Cr(VI), and Freundlich adsorption isotherms for (c) As(III) and (d) Cr(VI) on Al-containing ferrihydrites.

Table 1
Isotherm parameters for adsorption of As(III) or Cr(VI) on Al-containing ferrihydrites.

Contaminants	Samples	Langmuir			Freundlich		
		q_m ($\mu\text{mol/g}$)	K_L ($\text{L}/\mu\text{mol}$)	R^2	K_F ($\mu\text{mol/g}(\text{L}/\mu\text{mol})^{1/n}$)	n	R^2
As(III)	Fh-Al-0	1234.1	0.0106	0.9886	133.8	3.061	0.9272
	Fh-Al-10	1056.7	0.0079	0.9952	100.9	2.988	0.9513
	Fh-Al-20	875.7	0.0091	0.9888	112.6	3.465	0.9356
	Fh-Al-30	867.1	0.0080	0.9847	102.7	3.360	0.9288
Cr(VI)	Fh-Al-0	805.1	0.3021	0.9915	420.0	11.276	0.9502
	Fh-Al-10	840.9	0.2746	0.9863	395.4	9.611	0.9801
	Fh-Al-20	852.1	0.4455	0.9887	421.9	10.269	0.9782
	Fh-Al-30	934.1	0.3722	0.9822	429.7	9.207	0.9799

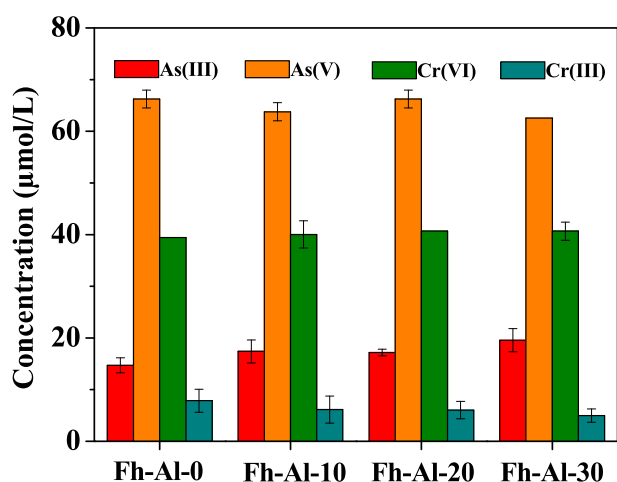


Fig. 5. The concentrations of As(III), As(V), Cr(VI) and Cr(III) desorbed from the four pre-adsorbed samples (1.0 mol/L NaOH were used as desorption solution).

be found that Fe, Al, O, As, and Cr elements exhibited similar mapping, covering the surface of this sample. Fe, and O were the main elements of ferrihydrite, while the occurrence of Al indicated that Al was successfully incorporated into ferrihydrite. Besides, the As and Cr elements were also detected, which indicated that As(III) and Cr(VI), as well as the generated As(V) and Cr(III) had been adsorbed on the surface of Fh-Al-30. The TEM image and its corresponding TEM-EDS elemental maps for Fh-Al-0 after reaction were also collected and discussed (Fig. S7).

3.6.2. ATR-FTIR

Fig. S8(a) displays ATR-FTIR data obtained from Fh-Al-30 before and after exposed to a mixture solution containing 150 $\mu\text{mol/L}$ As(III) and 100 $\mu\text{mol/L}$ Cr(VI) at pH 3.0. The spectra of original sample showed no obvious peak in the range of 750–950 cm^{-1} , while a peak at about 825 cm^{-1} appeared in the spectra after the Fh-Al-30 had been exposed to As(III) and Cr(VI) solution. According to the study by Cerkez et al. (2015), the peak at about 780, 820, and 920 cm^{-1} in ATR-FTIR spectra can be associated with adsorbed

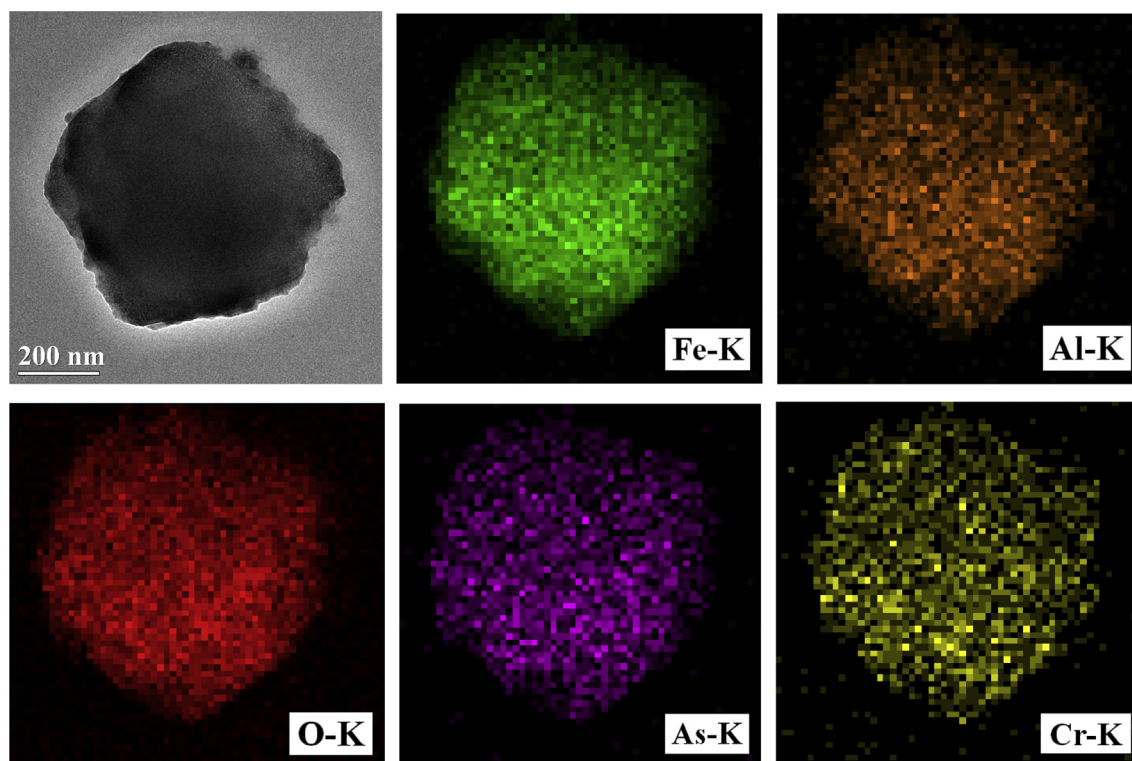


Fig. 6. TEM image and its corresponding TEM-EDS elemental maps for Fh-Al-30 after reaction.

As(III), As(V), and Cr(VI), respectively. In Fig. S8(a), the peak at about 825 cm^{-1} indicated the presence of As(V), while the absence of peak at about 780 cm^{-1} may be attributed to the fact that most As(III) was oxidized to As(V). Similar to As(III), the absence of peak at 920 cm^{-1} may be attributed to the fact that most Cr(VI) was reduced to Cr(III). Therefore, it is proposed that the redox conversion occurred between As(III) and Cr(VI) after the two contaminants were coadsorbed on Al-containing ferrihydrite. The ATR-FTIR analysis of Fh-Al-0 before and after reaction are also carried out and discussed in Fig. S8(b).

3.6.3. XPS

The compositions and oxidation states of Al-containing ferrihydrite before and after reaction with As(III) and Cr(VI) were

determined using XPS analysis techniques. Fig. 7(a) shows the high-resolution XPS spectra for Fe 2p of Fh-Al-30 before and after reaction. The Fe 2p lines of the two samples are similar, where the binding energy at 711.2 and 724.8 eV can be attributed to Fe $2p_{3/2}$ and Fe $2p_{1/2}$ of Fe(III) (Liu et al., 2016b), respectively. The high-resolution XPS spectra for Al 2p of Fh-Al-30 before and after reaction showed a characteristic peak at about 73.9 eV (Fig. 7(b)), indicating the oxidation state of Al(III) (Feng et al., 2014).

As shown in Fig. 7(c) and (d), O 1s signal of the two samples can be deconvoluted into three peaks. According to previous studies (Shahwan et al., 2011; Tang et al., 2013; Hien et al., 2014; Yan et al., 2015; Qi et al., 2016), the peaks at 529.4–530.3 eV, 530.6–531.4 eV, and 532.4–532.8 eV can be assigned to O in metal oxide (M-O), hydroxyl bonded to metal (M-OH), and adsorbed H_2O , respectively.

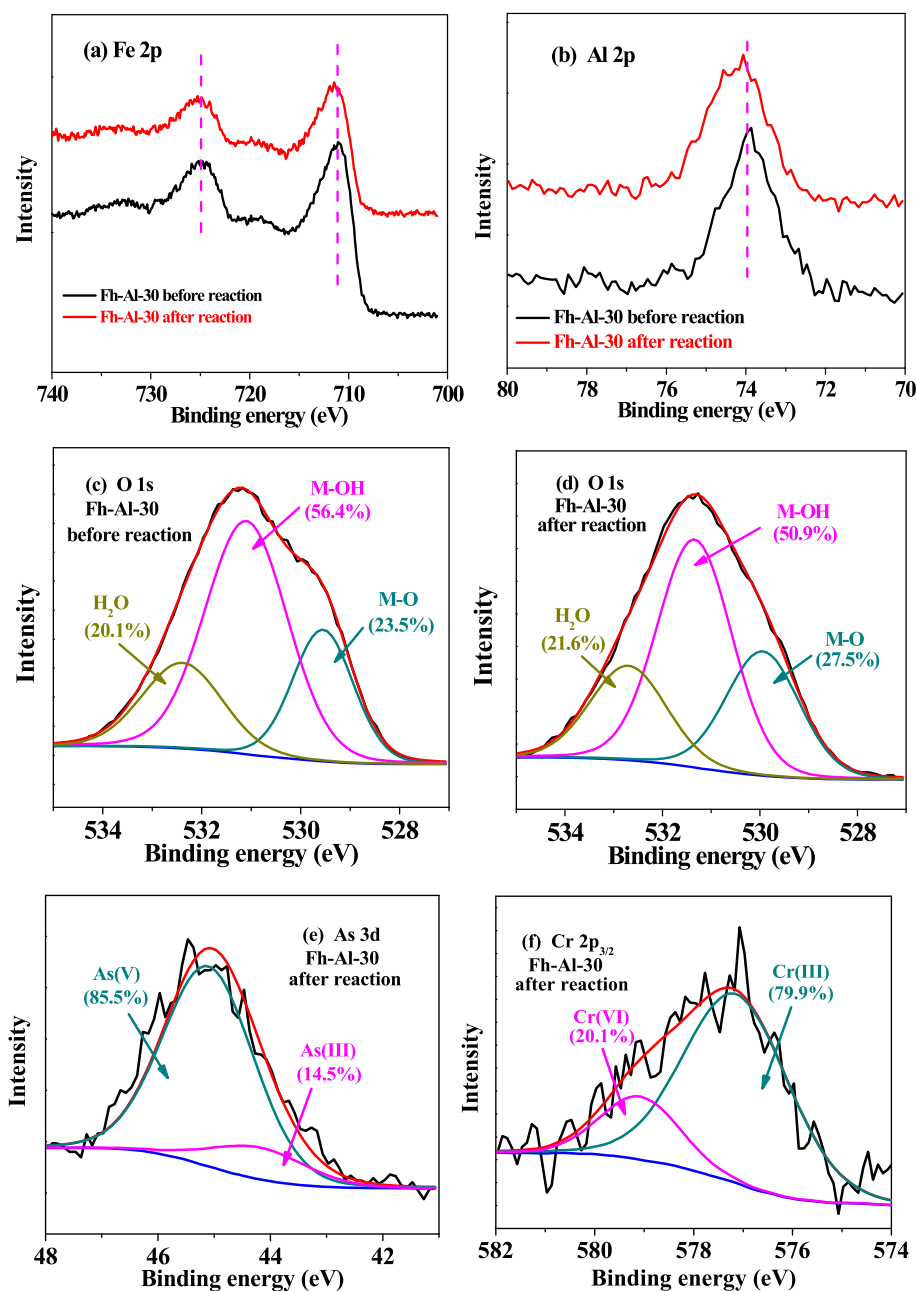


Fig. 7. (a) Fe 2p and (b) Al 2p spectra of Fh-Al-30 before and after reaction, O 1s spectra of Fh-Al-30 (c) before and (d) after reaction, (e) As 3d spectra and (f) Cr $2p_{3/2}$ spectra of Fh-Al-30 after reaction.

The results show that Fh-Al-30 possesses a high percentage of M-OH, which is a favorable factor for the immobility of As(III) and Cr(VI) (Ren et al., 2011; Johnston and Chrysochoou, 2015). After reaction with the two contaminants, the percentage of M-OH decreases from 56.4% to 50.9% for Fh-Al-30. According to the Eqs. (5) and (6), the decrease of M-OH percentage can be attributed to the complexation between M-OH and As(III), as well as between M-OH and Cr(VI). On the other hand, the percent fractions of M-O and H₂O increase after Fh-Al-30 reacted with the two contaminants. The increase of M-O percent fraction can be explained by the new O obtained from M-O-As and M-O-Cr after As(III) and Cr(VI) were adsorbed on the surface of Fh-Al-30. In addition, H₂O was generated during the complexation between M-OH and As(III), as well as between M-OH and Cr(VI), which can result in an increase of H₂O percentage.

High-resolution As 3d and Cr 2p_{3/2} spectra of Fh-Al-30 after reaction are shown in Fig. 7(e) and (f), respectively. It can be found that As 3d line of Fh-Al-30 after reaction can be fitted into two peaks at 44.2 and 45.1 eV. According to previous studies (Du et al., 2013; Yang et al., 2016), the binding energy of As(V) was 44.9 or 45.1 eV, higher than that of As(III), which was 44.2 eV. Therefore, it can be inferred that As(III) was mainly oxidized to As(V) after adsorption, and the percentage of As(III) oxidation is approximately 85.5%. Meanwhile, the Cr 2p_{3/2} spectra can be fitted by a characteristic peak of Cr(III) at 577.1 eV and a characteristic peak of Cr(VI) at 579.1 eV (Li et al., 2017). As shown in Fig. 7(f), approximately 79.9% of Cr(VI) was reduced to Cr(III). The percentage of As(III) oxidation is close to the percentage of Cr(VI) reduction, which indicates that the redox transformation occurred between As(III) and Cr(VI) after the two contaminants were coadsorbed on Fh-Al-30. While the dissolved oxygen (Fig. S5) in the reaction systems contributed to partial oxidation of As(III), resulting in a little higher As(III) oxidation percentage than Cr(VI) reduction percentage. Prior studies (Becker et al., 2001; Rosso and Becker, 2003; Cerkez et al., 2015) have reported that small band gap semiconductors, such as ferrihydrite, can play a role as conduits for electron transfer from a donor to acceptor. It is likely that Al-containing ferrihydrite works as conduits for electron transfer from As atoms to Cr atoms, resulting in the formation of As(V) and Cr(III).

The compositions and oxidation states of Fh-Al-0 before and after reaction with As(III) and Cr(VI) were also determined using XPS analysis techniques and discussed in Fig. S9.

3.7. Removal mechanism of As(III) and Cr(VI)

According to the above discussion, the removal of As(III) and Cr(VI) by Al-containing ferrihydrite is a complex process, including coadsorption and redox conversion behaviors (Fig. 8). First, both As(III) and Cr(VI) can be adsorbed onto the surface of Al-containing ferrihydrite due to electrostatic interaction and complexation with surface -OH. After the adsorption of As(III) and Cr(VI), M-O-As and M-O-Cr (where M represents Fe or Al) complexes on the surface of Al-containing ferrihydrite formed. The electron may transfer from the As atoms of M-O-As to M, pass through the solid phase of Al-containing ferrihydrite, and finally reach the Cr atoms of M-O-Cr, thus leading to the oxidation of As(III) to As(V) and the reduction of Cr(VI) to Cr(III).

4. Conclusions

In this study, large surface area Al-containing ferrihydrite is a high-efficiency adsorbent for As(III) and Cr(VI) under acidic and neutral conditions. With the increase of Al content in ferrihydrite, the adsorption capacity decreased for As(III), whereas it increased slightly for Cr(VI). The presence of Al in ferrihydrite decreased the affinity of ferrihydrite towards As(III), but increased the affinity towards Cr(VI). For Cr(VI), its removal efficiency was evidently dependent on pH, and Al-containing ferrihydrite achieved a high adsorption efficiency for Cr(VI) under acidic conditions and a low adsorption efficiency under alkaline conditions. For As(III), its decreasing rate was accelerated with the increase of pH from 3.0 to 7.0. However, when the pH increased to 11.0, As(III) decreasing rate slowed down. This effect of pH on As(III) removal may be attributed to the electrostatic interaction between As(III) and Al-containing ferrihydrite. Interestingly, it was found that the oxidation of As(III) to As(V) and reduction of Cr(VI) to Cr(III) occurred after the coadsorption of As(III) and Cr(VI) onto the surface of Al-containing ferrihydrite. The As(III) is much more toxic than As(V), and Cr(VI) is much more toxic than Cr(III). The redox conversion between As(III) and Cr(VI) can greatly lower the environmental hazard of the two contaminants. Given the abundance of Al-containing ferrihydrite in nature, the discoveries in the study can improve our understanding of the environmental fate of the As(III) and Cr(VI), as well as other contaminants that may react with Al-containing ferrihydrite.

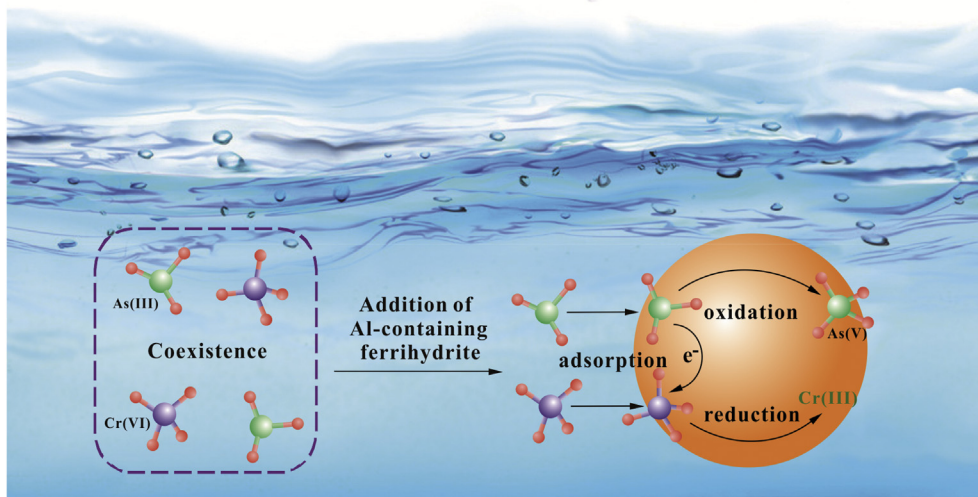


Fig. 8. Proposed mechanism of As(III) and Cr(VI) removal by Al-containing ferrihydrite.

Acknowledgements

This research was supported by National Natural Science Foundation of China (No. 51008084), Science and Technology Planning Project of Guangdong Province (No. 2016A020221032), Training Program for Outstanding Young Teachers in Guangdong Province (No. Yq2013055).

Appendix A. Supplementary data

Supplementary data related to this article can be found at <https://doi.org/10.1016/j.envpol.2017.12.118>.

References

- Adra, A., Morin, G., Ona-Nguema, G., Brest, J., 2016. Arsenate and arsenite adsorption onto Al-containing ferrihydrites. Implications for arsenic immobilization after neutralization of acid mine drainage. *Appl. Geochem.* 64, 2–9.
- Becker, U., Rosso, K.M., Hochella Jr., M.F., 2001. The proximity effect on semi-conducting mineral surfaces: a new aspect of mineral surface reactivity and surface complexation theory? *Geochim. Cosmochim. Acta* 65 (16), 2641–2649.
- Casey, W.H., 2006. Large aqueous aluminum hydroxide molecules. *Chem. Rev.* 106 (1), 1–16.
- Cerkez, E.B., Bhandari, N., Reeder, R.J., Strongin, D.R., 2015. Coupled redox transformation of chromate and arsenite on ferrihydrite. *Environ. Sci. Technol.* 49 (5), 2858–2866.
- Cismasu, A.C., Michel, F.M., Stebbins, J.F., Levard, C., Brown Jr., G.E., 2012. Properties of impurity-bearing ferrihydrite I. Effects of Al content and precipitation rate on the structure of 2-line ferrihydrite. *Geochim. Cosmochim. Acta* 92 (2), 275–291.
- Cismasu, A.C., Levard, C., Michel, F.M., Brown Jr., G.E., 2013. Properties of impurity-bearing ferrihydrite II: insights into the surface structure and composition of pure, Al- and Si-bearing ferrihydrite from Zn(II) sorption experiments and Zn K-edge X-ray absorption spectroscopy. *Geochim. Cosmochim. Acta* 119, 46–60.
- de Oliveira, L.M., Ma, L.Q., Santos, J.A.G., Guilherme, L.R.G., Lessl, J.T., 2014. Effects of arsenate, chromate, and sulfate on arsenic and chromium uptake and translocation by arsenic hyperaccumulator *Pteris vittata* L. *Environ. Pollut.* 184, 187–192.
- Du, Q., Zhang, S., Pan, B., Lv, L., Zhang, W., Zhang, Q., 2013. Bifunctional resin-ZVI composites for effective removal of arsenite through simultaneous adsorption and oxidation. *Water Res.* 47 (16), 6064–6074.
- Ekstrom, E.B., Learman, D.R., Madden, A.S., Hansel, C.M., 2010. Contrasting effects of Al substitution on microbial reduction of Fe(III) (hydr)oxides. *Geochim. Cosmochim. Acta* 74 (24), 7086–7099.
- Feng, L., Zhang, H., Wang, Z., Liu, Y., 2014. Superhydrophobic aluminum alloy surface: fabrication, structure, and corrosion resistance. *Colloids surf. A* 441, 319–325.
- Filip, J., Zboril, R., Schneeweiss, O., Zeman, J., Cernik, M., Kvapil, P., Otyepka, M., 2007. Environmental applications of chemically pure natural ferrihydrite. *Environ. Sci. Technol.* 41, 4367–4374.
- Fortin, D., Langley, S., 2005. Formation and occurrence of biogenic iron-rich minerals. *Earth Sci. Rev.* 72 (1–2), 1–19.
- Hien, V.X., You, J.L., Jo, K.M., Kim, S.Y., Lee, J.H., Kim, J.J., Heo, Y.W., 2014. H₂S-sensing properties of Cu₂O submicron-sized rods and trees synthesized by radio-frequency magnetron sputtering. *Sensor. Actuator. B Chem.* 202, 330–338.
- Jambor, J.L., Dutrizac, J.E., 1998. Occurrence and constitution of natural and synthetic ferrihydrite, a widespread iron oxyhydroxide. *Chem. Rev.* 98 (7), 2549–2586.
- Johnston, C.P., Chrysochoou, M., 2012. Investigation of chromate coordination on ferrihydrite by in situ ATR-FTIR spectroscopy and theoretical frequency calculations. *Environ. Sci. Technol.* 46, 5851–5858.
- Johnston, C.P., Chrysochoou, M., 2015. Mechanisms of chromate adsorption on boehmite. *J. Hazard Mater.* 281, 56–63.
- Johnston, C.P., Chrysochoou, M., 2016. Mechanisms of chromate, selenate, and sulfate adsorption on Al-substituted ferrihydrite: implications for ferrihydrite surface structure and reactivity. *Environ. Sci. Technol.* 50 (7), 3589–3596.
- Karapinar, N., 2016. Removal of heavy metal ions by ferrihydrite: an opportunity to the treatment of acid mine drainage. *Water Air Soil Pollut.* 227 (6), 1–8.
- Kim, K., Choi, W., 2011. Enhanced redox conversion of chromate and arsenite in ice. *Environ. Sci. Technol.* 45, 2202–2208.
- Kimbrough, D.E., Cohen, Y., Winer, A.M., Creelman, L., Mabuni, C., 1999. A critical assessment of chromium in the environment. *Crit. Rev. Environ. Sci. Technol.* 29 (1), 1–46.
- Kotaš, J., Stasicka, Z., 2000. Chromium occurrence in the environment and methods of its speciation. *Environ. Pollut.* 107 (3), 263–283.
- Le Hécho, I., Pecheyrat, C., Charles, S., Monperrus, M., Pavageau, M.P., Casiot, C., Potin-Gautier, M., Leblanc, M., Elbaz-Poulichet, F., Donard, O.F.X., 2003. Biogeochemical cycle and speciation of As and Cr in an acid mine environment: the case of Carnoules Creek, France. *J. Phys. IV* 107, 735–738.
- Levina, A., Codd, R., Dillon, C.T., Lay, P.A., 2003. Chromium in biology: toxicology and nutritional aspects. *Prog. Inorg. Chem.* 51, 145–250.
- Li, N., Fu, F., Lu, J., Ding, Z., Tang, B., Pang, J., 2017. Facile preparation of magnetic mesoporous MnFe₂O₄@SiO₂-CTAB composites for Cr(VI) adsorption and reduction. *Environ. Pollut.* 220, 1376–1385.
- Liu, J., Zhu, R., Xu, T., Xu, Y., Ge, F., Xi, Y., Zhu, J., He, H., 2016a. Co-adsorption of phosphate and zinc(II) on the surface of ferrihydrite. *Chemosphere* 144, 1148–1155.
- Liu, Y., Zhang, N., Yu, C., Jiao, L., Chen, J., 2016b. MnFe₂O₄@C nanofibers as high-performance anode for sodium-ion batteries. *Nano Lett.* 16 (5), 3321–3328.
- Martin, S., Zhu, C., Rule, J., Nuhfer, N.T., Ford, R., Hedges, S., Soong, Y., 2005. A high-resolution TEM-AEM, pH titration, and modeling study of Zn²⁺ coprecipitation with ferrihydrite. *Geochim. Cosmochim. Acta* 69 (6), 1543–1553.
- Meng, S., Wang, H., Liu, H., Yang, C., Wei, Y., Hou, D., 2014. Evaluation of the ability of ferrihydrite to bind heavy metal ions: based on formation environment, adsorption reversibility and ageing. *Appl. Geochem.* 45, 114–119.
- Michel, F.M., Ehm, L., Antao, S.M., Lee, P.L., Chupas, P.J., Liu, G., Strongin, D.R., Schoonen, M.A.A., Phillips, B.L., Parise, J.B., 2007. The structure of ferrihydrite, a nanocrystalline material. *Science* 316 (5832), 1726–1729.
- Nordstrom, D.K., 2002. Worldwide occurrences of arsenic in ground water. *Science* 296 (5576), 2143–2145.
- Qi, P., Pichler, T., 2016. Sequential and simultaneous adsorption of Sb(III) and Sb(V) on ferrihydrite: implications for oxidation and competition. *Chemosphere* 145, 55–60.
- Qi, L., Cheng, B., Yu, J., Ho, W., 2016. High-surface area mesoporous Pt/TiO₂ hollow chains for efficient formaldehyde decomposition at ambient temperature. *J. Hazard Mater.* 301, 522–530.
- Ren, Z., Zhang, G., Chen, J.P., 2011. Adsorptive removal of arsenic from water by an iron-zirconium binary oxide adsorbent. *J. Colloid Interface Sci.* 358 (1), 230–237.
- Rosso, K.M., Becker, U., 2003. Proximity effects on semiconducting mineral surfaces II: distance dependence of indirect interactions. *Geochim. Cosmochim. Acta* 67 (5), 941–953.
- Shahwan, T., Abu Sirriah, S., Nairat, M., Boyaci, E., Eroglu, A.E., Scott, T.B., Hallam, K.R., 2011. Green synthesis of iron nanoparticles and their application as a Fenton-like catalyst for the degradation of aqueous cationic and anionic dyes. *Chem. Eng. J.* 172 (1), 258–266.
- Smedley, P.L., Kinniburgh, D.G., 2002. A review of the source, behaviour and distribution of arsenic in natural waters. *Appl. Geochem.* 17 (5), 517–568.
- Smith, S.J., Page, K., Kim, H., Campbell, B.J., Boerio-Goates, J., Woodfield, B.F., 2012. Novel synthesis and structural analysis of ferrihydrite. *Inorg. Chem.* 51 (11), 6421–6424.
- Sorg, T.J., Chen, A.S.C., Wang, L., 2014. Arsenic species in drinking water wells in the USA with high arsenic concentrations. *Water Res.* 48, 156–169.
- Tang, W., Su, Y., Li, Q., Gao, S., Shang, J.K., 2013. Superparamagnetic magnesium ferrite nanoadsorbent for effective arsenic (III, V) removal and easy magnetic separation. *Water Res.* 47 (11), 3624–3634.
- Tang, L., Feng, H., Tang, J., Zeng, G., Deng, Y., Wang, J., Liu, Y., Zhou, Y., 2017. Treatment of arsenic in acid wastewater and river sediment by Fe@Fe₂O₃ nanobunches: the effect of environmental conditions and reaction mechanism. *Water Res.* 117, 175–186.
- Yan, Z., Xu, Z., Yu, J., Jaroniec, M., 2015. Highly active mesoporous ferrihydrite supported Pt catalyst for formaldehyde removal at room temperature. *Environ. Sci. Technol.* 49 (11), 6637–6644.
- Yang, Z., Shan, C., Zhang, W., Jiang, Z., Guan, X., Pan, B., 2016. Temporospatial evolution and removal mechanisms of As(V) and Se(VI) in ZVI column with H₂O₂ as corrosion accelerator. *Water Res.* 106, 461–469.
- Zhang, G., Qu, J., Liu, H., Liu, R., Wu, R., 2007. Preparation and evaluation of a novel Fe-Mn binary oxide adsorbent for effective arsenite removal. *Water Res.* 41 (9), 1921–1928.
- Zhao, Z., Jia, Y., Xu, L., Zhao, S., 2011. Adsorption and heterogeneous oxidation of As(III) on ferrihydrite. *Water Res.* 45 (19), 6496–6504.
- Zhou, T., Wu, X., Mao, J., Zhang, Y., Lim, T.T., 2014. Rapid degradation of sulfonamides in a novel heterogeneous sonophotocatalytic magnetite-catalyzed Fenton-like (US/UV/Fe₃O₄/oxalate) system. *Appl. Catal. B Environ.* 160–161, 325–334.
- Zhu, J., Pigna, M., Cozzolino, V., Caporale, A.G., Violante, A., 2011. Sorption of arsenite and arsenate on ferrihydrite: effect of organic and inorganic ligands. *J. Hazard Mater.* 189 (1–2), 564–571.